Micromagnetic three-dimensional simulation of the pinning field in high temperature $Sm(Co,Fe,Cu,Zr)_z$ magnets

W. Scholz,[a] J. Fidler, T. Schrefl, D. Suess, and T. Matthias
Institut für Angewandte und Technische Physik, Vienna University of Technology, Wiedner Hauptstrasse 8-10/137, A-1040 Vienna, Austria

We have investigated domain wall pinning in $Sm(Co,Fe,Cu,Zr)_z$ based magnets with 3D micromagnetic simulations using a hybrid finite element/boundary element method. Transmission electron micrographs of magnets with $Sm_2(Co,Fe)_{17}$ matrix and $Sm(Co,Cu)_{5-7}$ precipitation phases were used to model the cellular microstructure. The pinning field was investigated for varying thickness of the intercellular phase. © *2002 American Institute of Physics.*
[DOI: 10.1063/1.1453326]

In the 1960's Strnat and co-workers[1] discovered samarium-cobalt-type permanent magnets. The reason for the excellent magnetic properties of this material are the high magnetic moment of Sm and Co as well as the high magnetocrystalline anisotropy. The high Curie temperature of 720 °C for $SmCo_5$ and 820 °C for Sm_2Co_{17}[2] makes it the best material currently available for high temperature magnets.[3–5]

Precipitation hardened $Sm(Co,Fe,Cu,Zr)_{7.5-8}$ magnets are classified as "pinning controlled"[6,7] and their behavior arises from the cellular precipitation structure, which is observed in transmission electron micrographs. The magnetic properties are determined by the fine cell morphology with rhombohedral cells of $Sm_2(Co,Fe)_{17}$ with a typical diameter of 100–200 nm, which are separated by a boundary phase of $Sm(Co,Cu,Zr)_{5-7}$.[8] The cellular precipitation structure is formed during the isothermal aging procedure in the production process.[9] Its development is determined by the direction of zero deformation strains due to the lattice misfit between the different phases.[10] The cellular precipitates act as pinning sites for magnetic domain walls, which is observed in Lorentz electron micrographs.[9]

The difference in composition and crystal structure between the cells and the cell boundary phase gives rise to a difference in the magneto-crystalline anisotropy. As a result, it is energetically favorable for a magnetic domain wall to either stay in the cell boundary phase ("attractive domain wall pinning" if the domain wall energy is lower) or just inside the cells ("repulsive domain wall pinning" if the domain wall energy in the cell boundary phase is higher than that in the cells).[11]

A finite element model of the microstructure of $Sm(Co,Fe,Cu,Zr)_z$ has been developed. It consists of $2\times2\times2$ rhombohedral cells with a spacer layer for the cell boundary phase in between (see Fig. 1). The edge length e and the "corner angle" β of the rhombohedrons as well as the thickness t of the precipitation are variable. The "space diagonal" D is parallel to the easy axis. The domain wall of the initial magnetization distribution of our simulations lies in the plane, which is indicated by the thick lines.

We have assumed the following material parameters for 300 K:[2] For the cells ("2:17" type) $J_s=1.32$ T, $A=14$ pJ/m, $K_1=5$ MJ/m^3. For the cell boundary phase ("1:5" type) we have used $J_s=0.8$ T, $A=14$ pJ/m, $K_1=1.9$ MJ/m^3. The resulting exchange length is 1.7 nm in the cells and 2.7 nm in the cell boundary phase. Thus, the domain wall width is 5.3 nm in the cells and 8.5 nm in the cell boundary phase.

These material parameters with lower anisotropy in the intercellular phase as compared to the cells gives rise to "attractive pinning," which means, that the domain wall prefers to move into the intercellular phase and stays there pinned.

We have studied the influence of the material parameters by varying the anisotropy constant K_1 of the precipitation between 0.4 MJ/m^3 (to mimic almost isolated cells or a close to paramagnetic—Cu rich—intercellular phase, A and J_s have also been reduced) and the value for the cells. The demagnetization curves in Fig. 2 have been obtained for cells with $e=50$ nm and $\beta=60°$, which gives $D\approx125$ nm, and $t=5$ nm. For very low values of the anisotropy constant we find a very strong pinning effect (horizontal plateau in the demagnetization curve in Fig. 2). As K_1 approaches the value for the cells (2:17 phase) the pinning effect disappears.

If the magneto-crystalline anisotropy of the intercellular phase is larger than that of the cells, the second possible pinning mechanism is found: "repulsive pinning."

The demagnetization curves for repulsive pinning and different values of the anisotropy constant of the intercellular phase are shown in Fig. 3. For only slightly enhanced values of the anisotropy constant K_1 we find no pinning, but for $\Delta K_1\geqslant4.0$ MJ/m^3 the pinning field reaches 1.5 kA/m. In this regime the pinning field is directly proportional to ΔK_1. The results for attractive and repulsive pinning are summarized in Fig. 4.

However, not only the material composition and material parameters, but also the geometry of the cellular structure has an important influence on the magnetic properties. The influence of the cell size has been studied previously[12] and it showed a strong increase with increasing size of the cells (when the composition of the magnet was kept constant by increasing the cell boundary, too). We have investigated solely the influence of the thickness of the cell boundary phase on the domain wall pinning and the pinning field, but kept the cell size constant. This time we have used a larger

[a]Electronic mail: werner.scholz@tuwien.ac.at

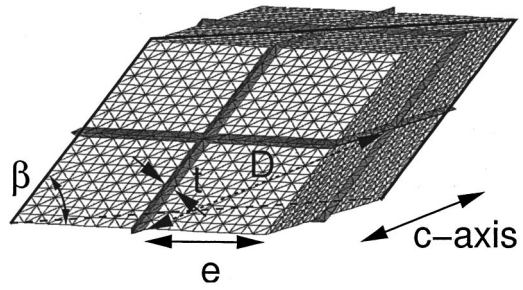

FIG. 1. Geometry of the finite element model.

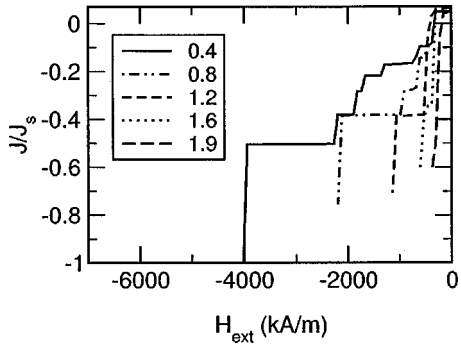

FIG. 2. Demagnetization curves for reduced magneto-crystalline anisotropy K_1 of the cell boundary phase (values in the legend in MJ/m^3)—attractive pinning.

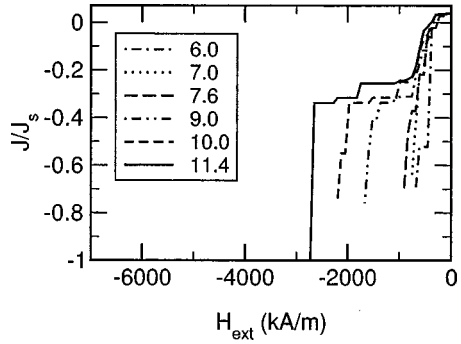

FIG. 3. Demagnetization curves for enhanced magneto-crystalline anisotropy K_1 of the cell boundary phase (values in the legend in MJ/m^3)—repulsive pinning.

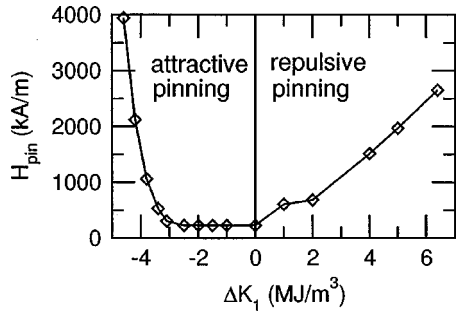

FIG. 4. Pinning field vs difference in anisotropy constant between the cells and the cell boundary phase.

TABLE I. The *z*-values for different thicknesses *t* of the cell boundary phase around cells with $D=250$ nm.

t (nm)	$V_{2:17}$ (nm^3)	$V_{1:5}$ (nm^3)	ratio	z
2.5	28 738	2 358	12.187	8.13
5	28 738	4 843	5.934	7.81
10	28 738	10 202	2.817	7.31
20	28 738	22 570	1.273	6.64
40	28 738	54 643	0.526	5.93

model of $3\times3\times3$ cells and larger cells with $e=100$ nm and $\beta=60°$, which gives $D\approx250$ nm. The thickness has been varied from $t=2.5$ nm to $t=40$ nm and the material parameters for the 2:17 cells and the 1:5 intercellular phase at 300 K given above have been used.

As we are varying the thickness, the ratio of the volume of the cells $V_{2:17}$ to the volume of the cell boundary phase $V_{1:5}$ changes. Thus, the composition and the *z* value change. These data are summarized in Table I, where a volume of $V_e^{2:17}=0.248\,53$ nm^3 and $V_e^{1:5}=0.0859$ nm^3 for the elementary cells of the 2:17-type cells and the 1:5-type cell boundary phase, respectively, have been assumed.[13] The *z* value is determined by

$$z=\frac{17\cdot V_{2:17}/V_e^{2:17}+5\cdot V_{1:5}/V_e^{1:5}}{2\cdot V_{2:17}/V_e^{2:17}+1\cdot V_{1:5}/V_e^{1:5}},$$

where all additives have been neglected.

The demagnetization curves given in Fig. 5 show, that for a very thin cell boundary phase (2.5 nm, 5 nm), the effect of domain wall pinning vanishes, because the domain wall width is larger than the thickness of the cell boundary phase. For a thickness of 10 and 20 nm we find strong domain wall pinning. When an external field of about 2500 kA/m is applied, the domain wall can overcome the energy barrier and cross the cell boundary phase. For a cell boundary phase with a thickness of more than four times the domain wall width, the analysis of the magnetization distribution reveals a new behavior: The whole cell boundary phase reverses starting from the original position of the domain wall, because the curvature of the domain wall[14] allows it to propagate through the whole cell boundary phase. Thus, the pinning field and the coercivity are reduced. The reversal of the whole intercellular phase leads to the second plateau in the demagnetization curve for $t=40$ nm in Fig. 5. Only at

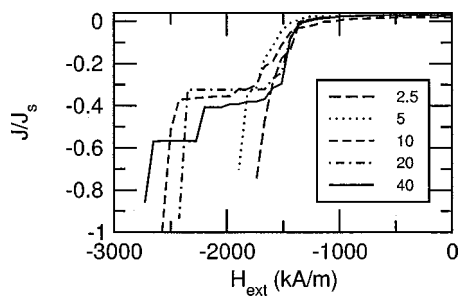

FIG. 5. Demagnetization curves for varying thicknesses *t* (values in the legend in nm) of the intercellular phase around large cells with $D=250$ nm.

higher fields the magnetization reversal of the cells starts with the nucleation of a reversed domain in a corner of the rhombohedral cells.

Due to pinning on the computational grid[15] an external field of 1500 kA/m is required to move the domain wall from its initial position. This effect has to be attributed to the size of the large model with $3\times3\times3$ cells, the larger size of the cells and the lower resolution of the finite element mesh. However, it has been verified that similar pinning fields are obtained for the smaller model.

In order to improve the magnetic properties of pinning controlled $Sm(Co,Fe,Cu,Zr)_z$ magnets, the thickness and the composition of the cell boundary phase have to be optimized. As the difference between the anisotropy constants of the cells and the cell boundary phase increases, the pinning field and, as a result, the coercive field of the magnet increase in the regime of attractive as well as in that of repulsive pinning. However, our simulations show that the thickness of the cell boundary phase plays a crucial role for attractive domain wall pinning, since it must not be too thin, for the domain wall to ''fit in'' and it must not be thicker than four times the domain wall width.

This work is supported by the EC Project HITEMAG (GRD1-1999-11125).

[1] K. J. Strnat, G. Hoffer, J. Oson, and W. Ostertag, J. Appl. Phys. **38**, 1001 (1967).
[2] K.-D. Durst, H. Kronmüller, and W. Ervens, Phys. Status Solidi A **108**, 403 (1988).
[3] M. S. Walmer, C. H. Chen, and M. H. Walmer, IEEE Trans. Magn. **36**, 3376 (2000).
[4] M. Corte-Real, Z. Chen, H. Okumura, and G. Hadjipanayis, IEEE Trans. Magn. **36**, 3306 (2000).
[5] S. Liu, J. Yang, G. Doyle, G. Potts, and G. E. Kuhl, J. Appl. Phys. **87**, 6728 (2000).
[6] K. J. Strnat, in *Ferromagnetic Materials*, edited by E. P. Wohlfarth and K. H. J. Buschow (North-Holland, Amsterdam, 1988), Vol. 4, pp. 131–209.
[7] K. D. Durst and H. Kronmüller, in *Proceedings of the Eighth International Workshop on Rare-Earth Magnets and Their Applications and the Fourth International Symposium on Magnetic Anisotropy and Coercivity in Rare Earth-Transition Metal Alloys*, edited by K. J. Strnat (University of Dayton, Dayton, OH, 1985), pp. 725–735.
[8] H. Kronmüller, in *Proceedings of the 6th International Workshop on Rare Earth-Cobalt Permanent Magnets and Their Applications and 3rd International Symposium on Magnetic Anisotropy and Coercivity in Rare Earth-Transition Metal Alloys*, edited by J. Fidler (Tech. University of Vienna, Vienna, Austria, 1985), pp. 555–565.
[9] G. C. Hadjipanayis, W. Tang, Y. Zhang, S. T. Chui, J. F. Liu, C. Chen, and H. Kronmüller, IEEE Trans. Magn. **36**, 3382 (2000).
[10] J. D. Livingston and D. L. Martin, J. Appl. Phys. **48**, 1350 (1977).
[11] W. Tang, Y. Zhang, A. M. Gabay, M. F. de Campos, and G. C. Hadjipanayis, J. Magn. Magn. Mater. (submitted).
[12] B. Streibl, J. Fidler, and T. Schrefl, J. Appl. Phys. **87**, 4765 (2000).
[13] E. Estevez-Rams, Dissertation, TU Vienna, 1996.
[14] R. Skomski, J. Appl. Phys. **81**, 5627 (1997).
[15] M. J. Donahue and R. D. McMichael, Physica B **233**, 272 (1997).